Expanded View Figures

Figure EV1. SEC-SAXS analysis of ABK complex.

A–C Experimental profiles (A), Guinier plots (B) and dimensionless Kratky plots (C) of the SAXS measurements of ABK comparing the ascent and decent sides of the peak. The chromatogram results show that the R_g between the ascent and descent sides of the peak are different. The shape of the scattering profile on the ascent side of the peak differs from that of the descent side of the peak, where the R_g value is stable. Guinier plot indicates a rise of the scattering profile on the small angle region. Based on the above results, the ascent side of the peak contains an oligomeric component, making it difficult to obtain a single structure. Thus, we calculated the structure using only the descent side of the peak.

D Results of the DAMMIF modeling of ABK using the data from the descent side of the peak. The DAMMIF process involved calculating 20 individual structural models, which were then superimposed and analyzed using cluster analysis. One of the structures was excluded from subsequent calculations based on the normalized spatial discrepancy (NSD) score obtained during the superimposition process. Consequently, the remaining 19 models are presented. All the structures obtained here exhibited a characteristic formation of a C-shaped upper part and a rod-like lower part. These structures were averaged, and the excess portions of each structure relative to the average structure were filtered out to create an initial structure. This initial structure was used for the final DAMMIN calculation. The resulting structure from this process was considered as the final model.

E Docking simulation of APC armadillo-repeat domain and β-catenin structures (PDB codes: 3NMZ and 1I7X) into the possible cargo-binding cavity of the ABK SAXS model. ABK: KIF3-ACT/BCT/KAP3 complex.

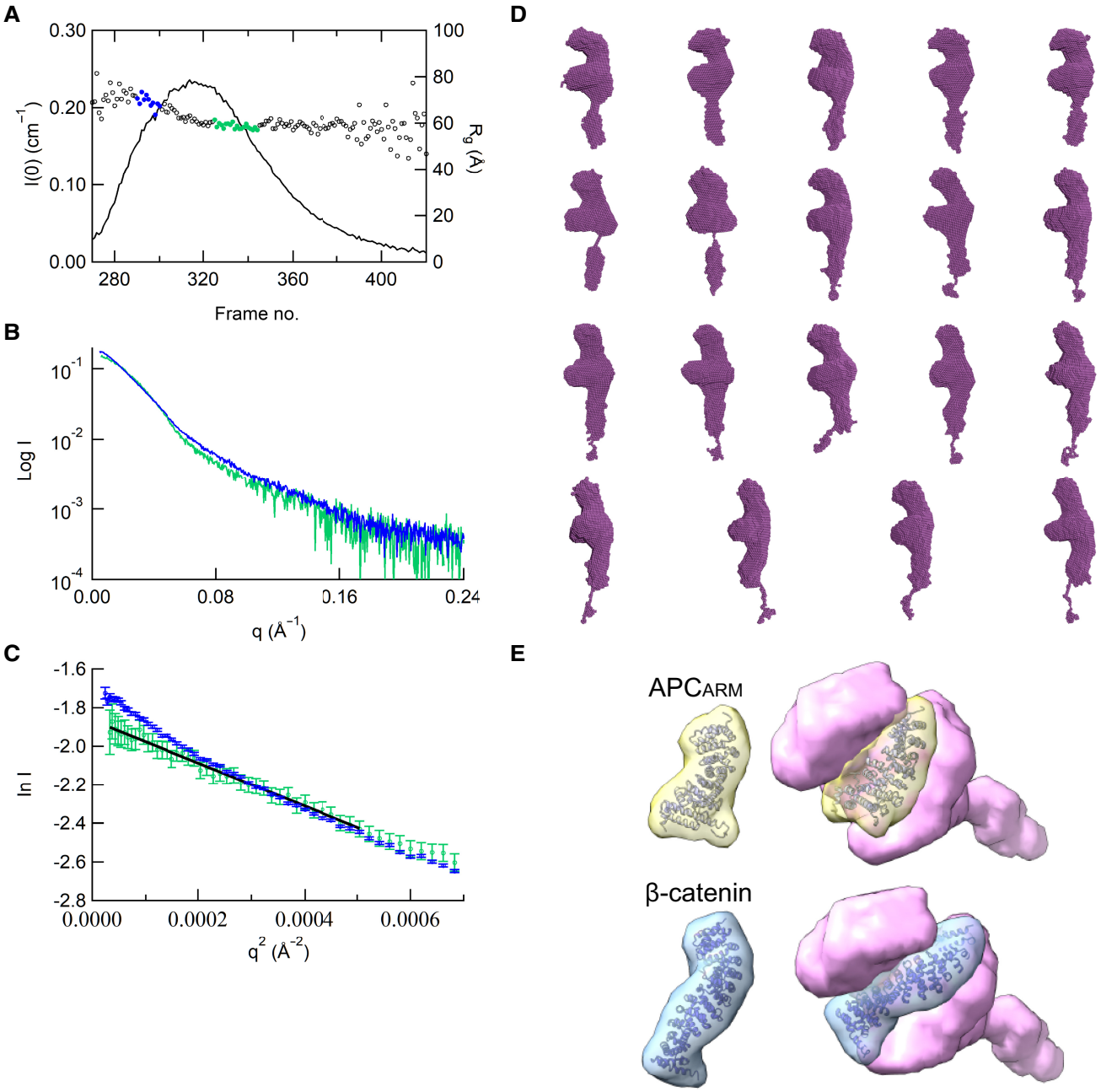

Figure EV1.

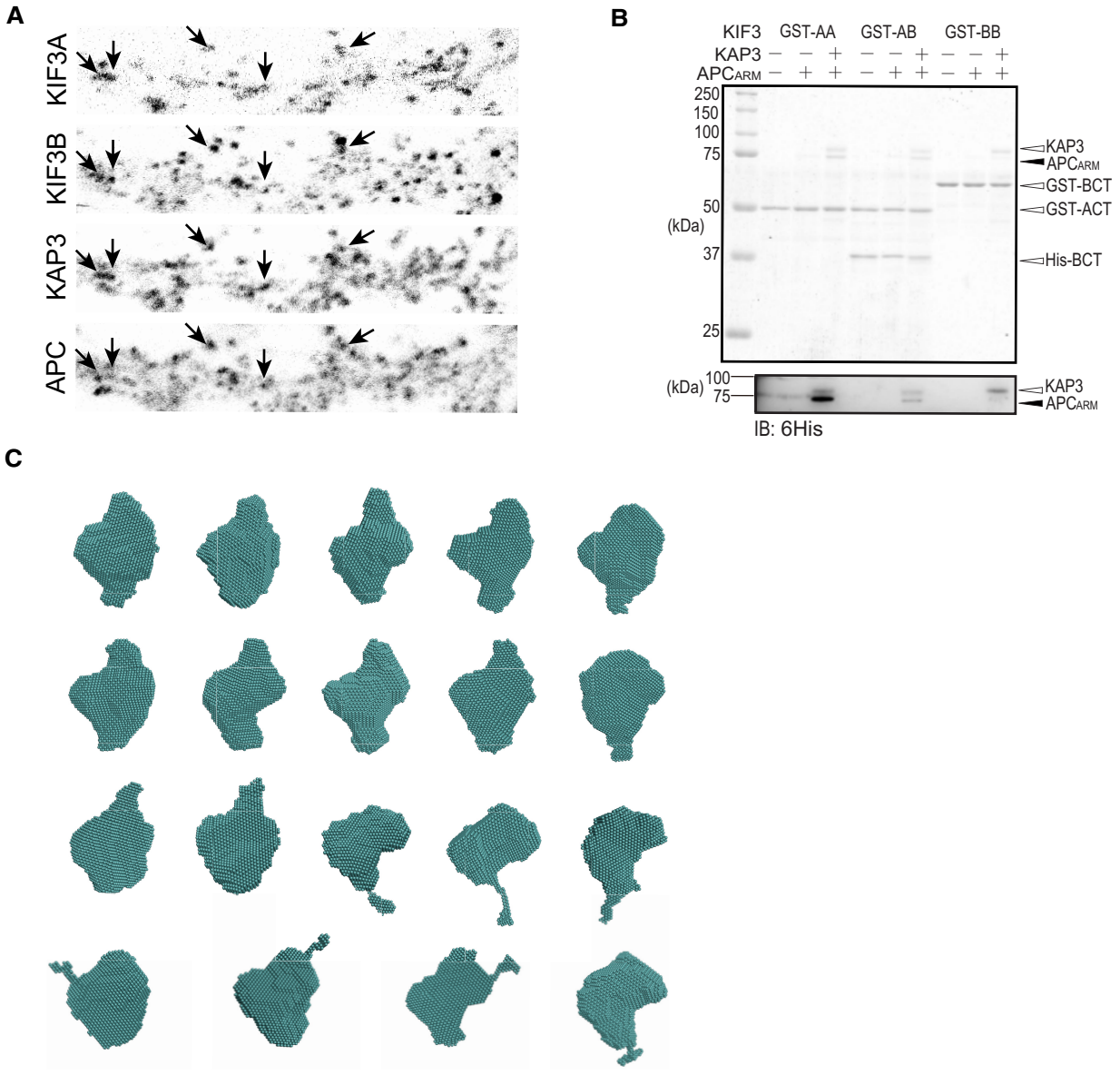

Figure EV2. Binding analysis of KIF3A/B/KAP3 with APC and DAMMIF modeling of ABK-APC$_{ARM}$ complex.

A Representative images of the immunostaining of KIF3A, KIF3B, KAP3 and APC in the dendrite region of hippocampal primary neurons. Arrows indicate representative colocalizations between KIF3A/B/KAP3 complex and APC. Images shown here are used to generate merged images in Fig 2A.

B Pull-down assay assessing the binding capability of KIF3/KAP3 complexes with APC$_{ARM}$. GST-AA, GST-BB, and GST-AB indicate the GST-tagged homodimeric ACT (KIF3A 481–701), homodimeric BCT (KIF3B 472–747), and heterodimeric ACT/BCT, respectively. The results were evaluated by CBB staining (top panel), and Western blot (bottom panel) using an anti-6His antibody to probe His-tagged KAP3 and APC$_{ARM}$.

C Results of the DAMMIF modeling of ABK-APC$_{ARM}$. The DAMMIF process involved calculating 20 individual structural models, which were then superimposed and analyzed using cluster analysis. One of the structures was excluded from subsequent calculations based on the NSD score obtained during the superimposition process. Consequently, the remaining 19 models are presented. The molecular shapes obtained here all exhibit approximately spherical structures. These structures were averaged, and the excess portions of each structure relative to the average structure were filtered out to create an initial structure. This initial structure was used for the final DAMMIN calculation. The resulting structure from this process was considered the final model.

Figure EV3. XL-MS analysis of ABK-APC$_{ARM}$ complex.

XL-MS results in addition to those shown in Fig 3D. Intra indicates intramolecular crosslinking.

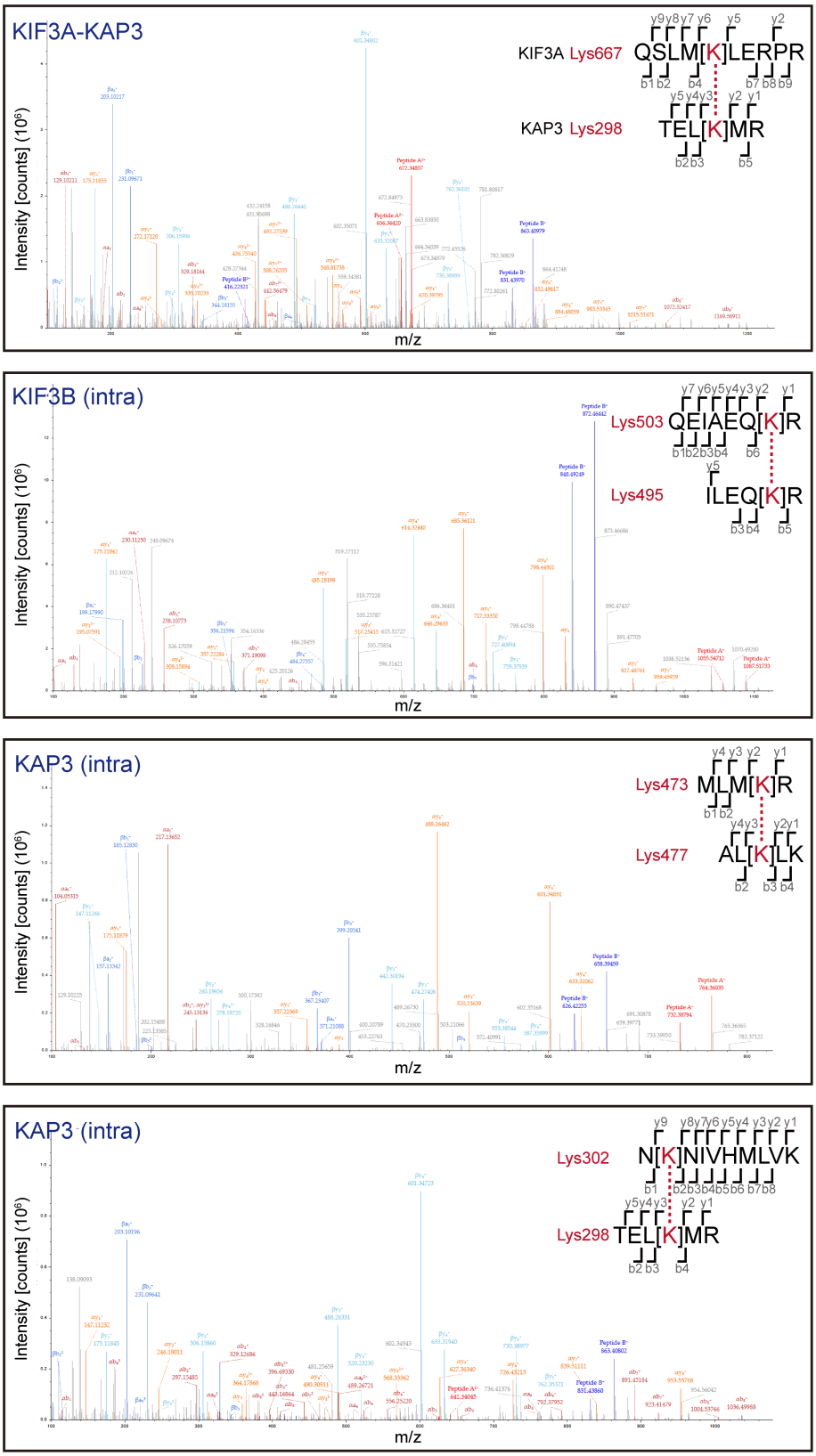

Figure EV3.

Figure EV4. HS-AFM analysis of ABK and BBK complexes.

A, B HS-AFM observation and representative particle images of ABK.
C Time lapse HS-AFM images of a representative ABK particle.
D, E HS-AFM observation and representative particle images of BBK.
F Time lapse HS-AFM images of a representative BBK particle.
G Statistical analysis of the AFM-based ABK, BBK and ABK-APC_{ARM} particle conformations. Distance from the coiled coil distal tip to the docking domain (as shown in Fig 4D) was calculated and plotted against time. Data derived from each of the three movies were indicated by different colors. The dotted lines indicate the averages of each group. BBK: KIF3-BCT/BCT/KAP3 complex.

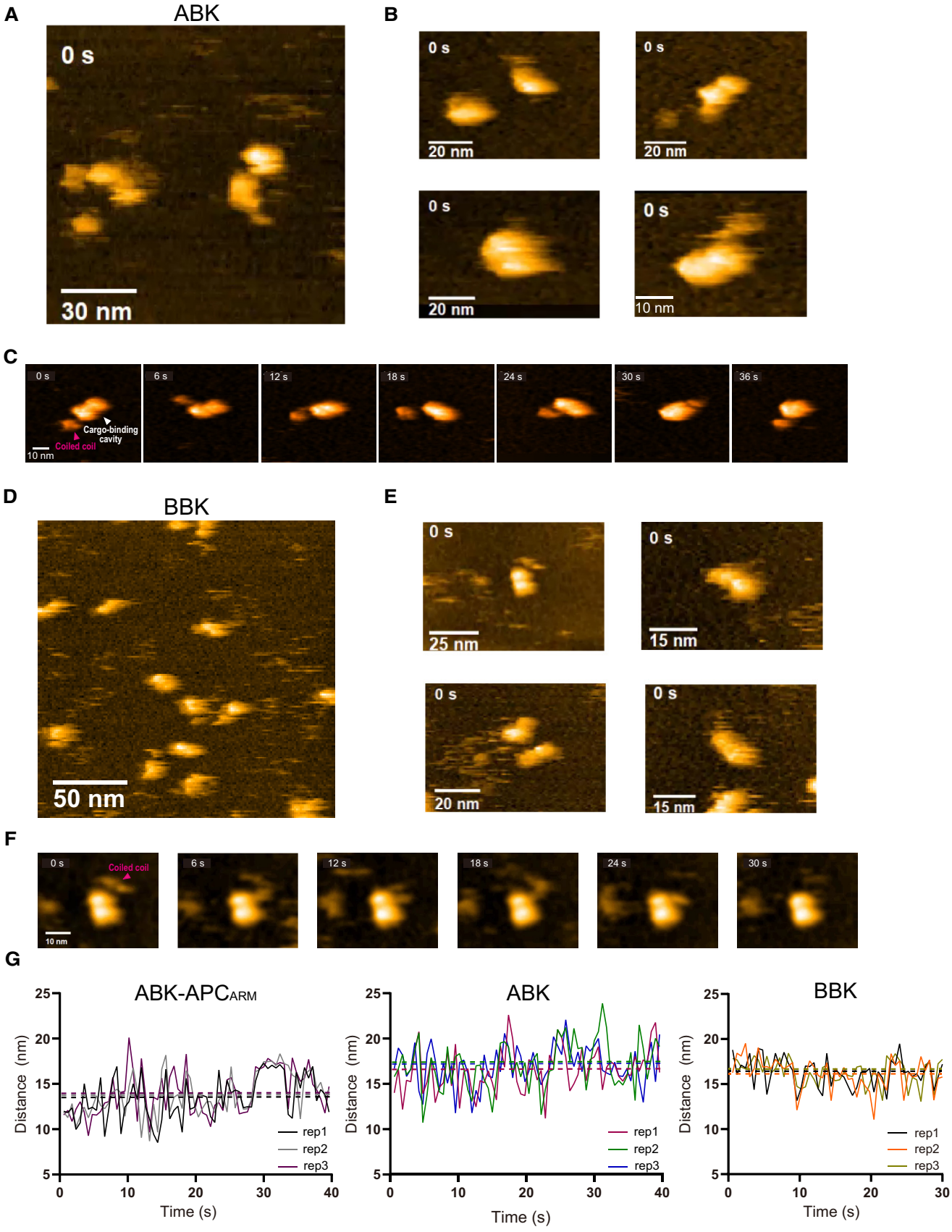

Figure EV4.

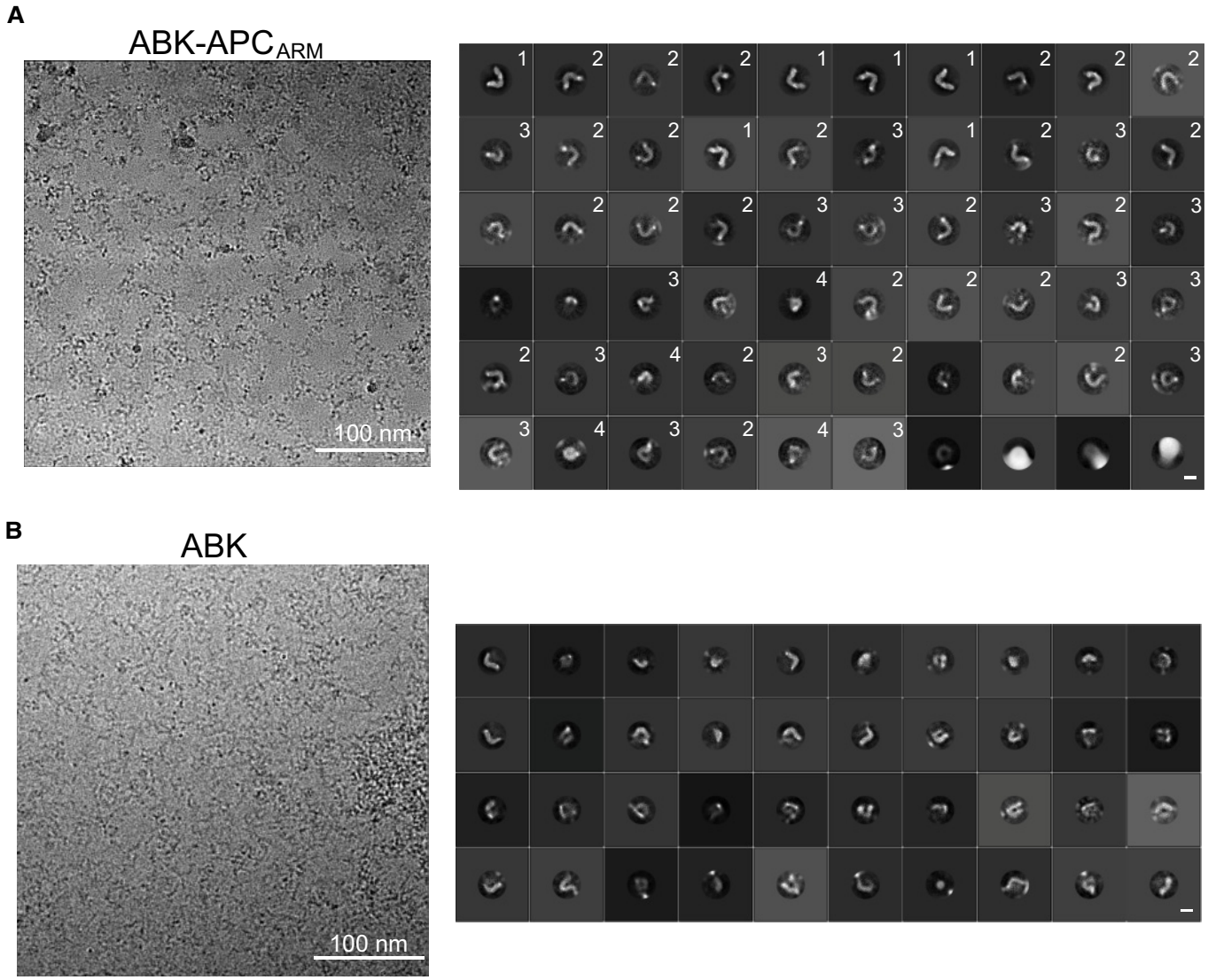

Figure EV5. CryoEM analysis of ABK and ABK$_{ARM}$ complexes.

A Left: representative cryoEM image of ABK-APC$_{ARM}$. Right: 2D class averages of ABK-APC$_{ARM}$ from cryoEM single particle analysis. 2D class averages were classified into four major groups with distinct conformations. HS-AFM observation and representative particle images of ABK-APC$_{ARM}$. Scale bars: 100 nm (left), 10 nm (right).

B Left: representative cryoEM image of ABK. Right: 2D class averages of ABK-APC$_{ARM}$ from cryoEM single particle analysis. Scale bars: 100 nm (left), 10 nm (right).